Modifying the Flexibility of Water Cages by Co-Including Acidic Species within Clathrate Hydrate

ARTICLE *in* THE JOURNAL OF PHYSICAL CHEMISTRY C · MARCH 2015

Impact Factor: 4.77 · DOI: 10.1021/jp511826b

THE JOURNAL OF PHYSICAL CHEMISTRY C

Article

pubs.acs.org/JPCC

Modifying the Flexibility of Water Cages by Co-Including Acidic Species within Clathrate Hydrate

Arnaud Desmedt,*[,†] Ludovic Martin-Gondre,[‡] The Thuong Nguyen,[†] Claire Pétuya,[†] Leyre Barandiaran,[†] Odile Babot,[†] Thierry Toupance,[†] R. Gary Grim,[§] and Amadeu K. Sum[§]

[†]Institut des Sciences Moléculaires, CNRS UMR5255 Université de Bordeaux, 351 cours de la Libération, F-33405 Talence, France

[‡]Université de Franche-Comté, UTINAM, CNRS UMR 6213, F-25030 Besançon, France

[§]Center for Hydrate Research, Chemical & Biological Engineering Department, Colorado School of Mines, 1500 Illinois Street, Golden, Colorado 80401, United States

ABSTRACT: Clathrate hydrates are crystalline materials made of water molecules forming host cages within which guest molecules are located. The hydrogen bond network ensuring the stability of the host substructure includes ionic defects, having an impact on the physicochemical properties of the systems. In this paper, a new way of introducing these ionic defects is proposed. Type II clathrate hydrates mixing tetrahydrofuran (THF) and perchloric acid guest molecules are synthesized and investigated by means of calorimetric, X-ray diffraction, and Raman scattering measurements together with a computational structure relaxation in the density functional theory approximation. The formation of the mixed clathrate hydrate with perchlorate anion included in the large cage of the cationic host-substructure of the THF type II clathrate hydrate requires the cooling of a (1-α) THF·$\alpha$$HClO_4$·17$H_2O$ solution with α less than 0.125. Above this inherent limitation, a multiphasic regime is observed in the formation of clathrate hydrate (mixture of type I and type II). The substitution of a THF molecule per perchlorate anion allows the modification of the melting of the type II clathrate hydrate, by preserving the clathrate structure. Shrinkage of the type II unit cell is measured together with a softening of the host lattice mode. In the harmonic approximation, the observation of both phenomena is counterintuitive and outline existing competition between anharmonicity of the cage energy landscape and ionic host−guest interaction. This study reveals the key role played by acidic defects existing in the host substructure on the physicochemical properties of clathrate hydrate.

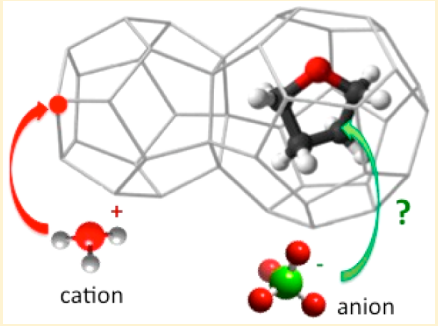

INTRODUCTION

Clathrate hydrates are supramolecular materials formed by the cocrystallization of at least one molecular species (guest) with water molecules (host), forming aqueous cages within which guest molecules are enclathrated.[1,2] Gas hydrates are probably one of the most fascinating systems, due to their importance in the broad area of energy.[2,3] Over the last few decades, ionic clathrate hydrates—i.e., obtained by incorporating ionic species—have gained interest, in particular related to the ionic add-ons supplied to various technological opportunities and with their specific physicochemical properties.[4]

Built upon the encapsulated molecules, clathrate hydrates involve various arrangements of the water cages.[2] These latter ones are formed from dynamically disordered hydrogen-bonded water molecules,[5] under the constraint of the so-called ice rule (i.e., each oxygen atom accepts and donates two H-bonds). The inclusion of ionic guest molecules (such as bases, strong acids, or quaternary ammonium salts) leads to form water substructure containing ionic defects, through the incorporation of counterions within the water framework. Such chemical defects in the clathrate hydrates lead to violation of the ice rule and thus modification of the intrinsic properties of the clathrate hydrates. For instance, their structural properties exhibit a large variability ranging from a semi-clathrate structure of quaternary ammonium salts[2] to a rich structural phase diagram depending on the hydration number as in the case of strong acids.[6−8] The thermodynamics of gas hydrates, such as their heat capacities, is modified by the addition of ionic species such as KOH[9] or ammonium salts.[10] Another striking properties in ionic clathrate hydrates made with alkyl ammonium hydroxide[11−13] or strong acids[7,14,15] is probably their superprotonic conductivity, due to a super-mobility of protons in the host substructure.[16−18] The modification of proton dynamics promoted by the addition of ionic species in the host substructure may also switch the thermal conductivity from an abnormal "glass-like" behavior to a standard crystalline behavior.[19] Finally, unusual properties of ionic clathrate hydrates are also outlined by their superoxide ion formation,[20] superexchange-like interaction,[21] or abnormal positioning of host molecules.[22]

In all cited examples, the key point triggering the properties is the existence of ionic defects within the host framework. To improve the knowledge of the impact of such defects, it is crucial to provide a way for generating them. The present paper

Received: November 26, 2014
Revised: March 25, 2015
Published: March 31, 2015

DOI: 10.1021/jp511826b
J. Phys. Chem. C 2015, 119, 8904−8911

addresses this issue and aims to investigate the impact of acidic defects on the basic physicochemical properties of clathrate hydrate. To study this, new mixed clathrate hydrates are considered by monitoring the insertion of acidic additives within a "standard" clathrate hydrate. The tetrahydrofuran (noted THF) clathrate hydrate has been selected as the "standard", since it probably represents a prototypical system, for which the thermodynamic, dynamical, structural, and promoter properties have been the subject of numerous studies.[2,5] Its clathrate hydrate structure ($THF{\cdot}17H_2O$ with a melting point at 277 K) is of type II with only the large cages filled with guest molecules.[23,24] The selected ionic system is the perchloric acid. Its most energetically stable clathrate hydrate phase is the type I structure ($HClO_4{\cdot}5.5H_2O$ with a melting point at 228 K) with perchlorate anions located within all cationic cages, thus constituted of water molecules and hydronium cations.[6] Both systems have been chosen because of the existing contrasts in terms of thermodynamics and structures, allowing the disentangling of any plausible multiphase phenomenon when both guest molecules are mixed to form the clathrate hydrate.

Thus, this paper reports the first investigation of a THF clathrate hydrate doped with ionic species—the perchloric acid. To unravel various properties of this new ionic clathrate hydrate, the thermodynamics (differential scanning calorimetry, DSC), structural (powder X-ray diffraction, PXRD), and vibrational properties (Raman scattering), in conjunction with density functional theory (DFT) structural relaxations, are presented in the following.

MATERIALS AND EXPERIMENTAL DETAILS

Experimental Measurements. Perchloric acid ($HClO_4$) aqueous solution (70% $HClO_4$) and 99.9% pure tetrahydrofuran (THF) solution were purchased from Sigma-Aldrich. Ultra high purity water (Milly Q quality) was used to prepare the solutions according to the following chemical formula, $(1-\alpha)THF{\cdot}\alpha\ HClO_4{\cdot}17H_2O$ with α ranging from 0 to 1/2. In the following, the clathrate hydrate formed by cooling a given solution is denoted with the corresponding α value.

The DSC experiments were performed on a PerkinElmer DSC 7. Temperature and heat flow were calibrated according to the melting point and fusion enthalpy of cyclohexane. The solutions were placed into a sealed gold cell. Cooling and heating cycles between 190 K and room temperature were performed at a rate of 5 °C/min.

PXRD was recorded with a Siemens D500 diffractometer with a Cu radiation source (Kristalloflex unit with a wavelength of 0.15418 nm) in the $\theta/2\theta$ scan mode. The beam size is about 0.4 mm × 12 mm. PXRD measurements were performed in the step-scan mode with a dwell time of 1.5 s and a step size of 0.02° on clathrate samples ground to a fine powder under liquid nitrogen and inert atmosphere. The sample powders were cold transferred into the PXRD stage, and all diffractograms were recorded in order of increasing temperatures between 150 K and room temperature. The PXRD pattern indexing and cell refinement were performed with PowderX[25] and Chekcell[26] programs.

Raman data were collected with a Labram microspectrometer (Horiba Jobin Yvon, Villeneuve d'Ascq, France) using a 485 nm ion Argon laser (Spectra Physics, France) as excitation source (power on samples at 30 mW). A 50× objective (NA = 0.45, Olympus) permitted us to focus the incident laser beam and to collect the Raman scattering. The Raman scattering was dispersed by a holographic grating of 1800 lines/mm and analyzed by a Peltier-cooled CCD detector (Andor, Belfast, UK), which permitted measuring simultaneously the intensity of different wavelengths of the spectrum with a spectral resolution better than 1 cm^{-1}. Calibration of the wavenumbers was done by using the 520.7 cm^{-1} mode of a silicon sample. The data were collected on a spectral range from 150 to 3800 cm^{-1}. The sample temperatures were maintained at the desired value (±1 K) during the acquisition by using a temperature-controlled stage (Linkam Scientific Instruments Ltd., UK).

Quantum Mechanics Calculations. DFT calculations were done with the Vienna *ab initio* simulation package (VASP) using plane-wave basis sets.[27,28] The exchange-correlation energy was calculated with the generalized gradient approximation GGA and the Perdew−Burke−Ernzerhof energy functional (PBE).[29] The electron−core interaction was described with the projector augmented-wave (PAW) method.[30,31] The energy cutoff in the plane-wave expansion was 520 eV corresponding to high precision VASP calculations. Because of the large size of the unit cells ($a \approx 17$ Å), all calculations were performed at the Γ point of the Brillouin zone.

The type II clathrate hydrates were generated in three steps. Initially, the oxygen positions of the aqueous structure were taken from X-ray diffraction data.[23] Two hydrogen atoms were then added to every oxygen atom to generate water molecules and to form hydrogen-bonded cages. Finally, all $5^{12}6^4$ cages were filled with a THF molecule placed in the cage center. The inclusion of perchloric acid was performed by substituting a THF molecule with a ClO_4^- anion, whereas the H^+ cation was added to adjacent oxygen atom to form a hydronium ion. When several acids molecules were included, they were homogeneously distributed in the unit cell. After the generation of the clathrate, a relaxation of atoms coordinates was required in order to determine the minimum energy structure. The structural optimization was a tricky task due to the large number of atoms (~500 atoms) involving a great number of degrees of freedom. As for the clathrate generation, three steps were considered to relax the structure. The first step consisted of relaxation of the hydrogen ions only in the aqueous structure. Then, the guest molecule geometry was optimized, and in a third step a global relaxation of all atoms was performed. All relaxations were based on a force convergence threshold of at least 0.02 eV/Å.

RESULTS

Differential Scanning Calorimetry. The measured thermograms of the THF clathrate hydrate (i.e., $\alpha = 0$) are shown in Figure 1. Cooling the solution leads to a single thermal anomaly while the heating cycle exhibits a complex thermal anomaly characterized with two melting peaks: the sample $THF{\cdot}17\ H_2O$ is then a mixture of ice and THF clathrate hydrate due to heterogeneous melting, in agreement with previous DSC results.[32] In addition, the shift in the baseline observed at the melting is known to be due to the existence of heat capacity prior to the melting,[33] finding its origin in structural modification observed above 250 K.[34,35] As shown in Figure 1, replacing a fraction of THF molecules with perchloric acid molecules yields the modification of the thermograms: the melting and fusion temperatures depend on the acid concentrations. On cooling the solution (Figure 1), DSC curves exhibit a single exothermic peak between ca. 230 and 255 K depending on the concentration of acids in the samples

DOI: 10.1021/jp511826b
J. Phys. Chem. C 2015, 119, 8904−8911

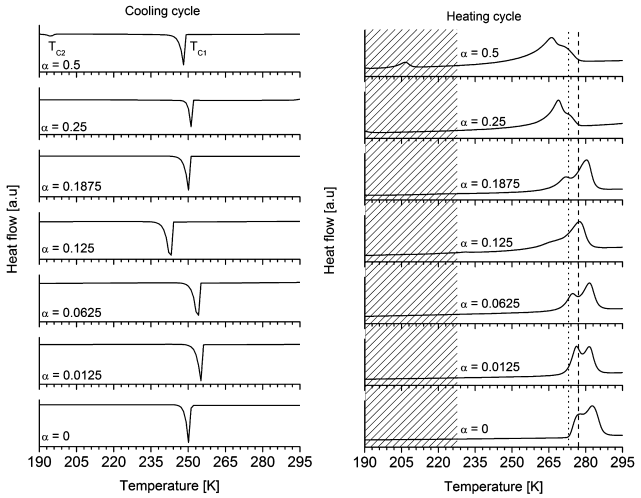

Figure 1. Differential scanning calorimetry curves of the mixed THF−$HClO_4$ clathrate hydrates for various acid concentrations α indicated on the figure. On the right side, the melting points of ice and THF·17 H_2O clathrate hydrate are indicated by the vertical dotted line and dashed line, respectively. The region in which the melting of the perchloric acid clathrate hydrate is expected is indicated by the filled pattern area.

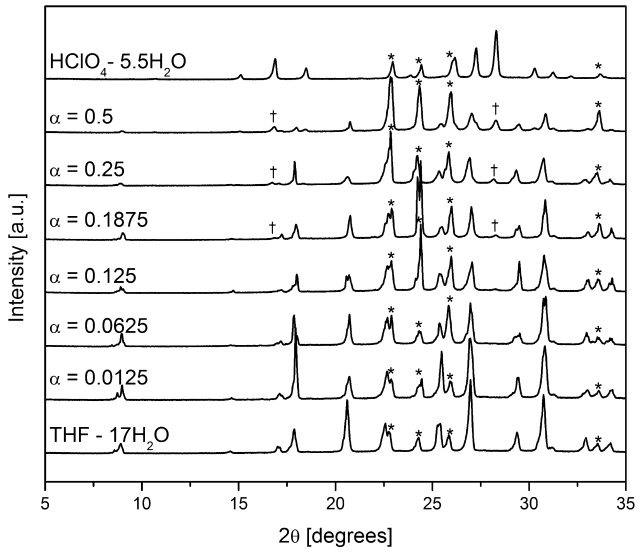

Figure 2. Diffractograms of the mixed THF−$HClO_4$ clathrate hydrates at 150 K for various acid concentrations α. The diffractogram recorded for the type I $HClO_4$·5.5 H_2O is also shown. The peaks indicated with crosses correspond to the type I clathrate hydrate structure. The ice Bragg peaks are indicated with asterisks.

(except for α = 0.5 as discussed hereafter). On heating the samples, two broad endothermic peaks are observed between 250 and 290 K (denoted T_{C1} transition). Such a double-peak feature is probably associated with a complex melting process as previously mentioned in the case of the pure THF clathrate hydrate. Moreover, for the highest acid concentration (i.e., α = 0.5), an additional weak thermal anomaly is observed at ca. 205 K (heating cycle) and at ca. 195 K (cooling cycle). Such a peak may then be associated with a structural phase transition observed at the highest acid concentration (denoted T_{C2} transition). Thus, the striking observations done on the DSC curves are (i) a double endothermic peak at the melting T_{C1}, (ii) a modification of the melting and fusion points depending on the acid concentration with minimum temperatures observed for α = 0.125, and (iii) the appearance of an additional structural phase transition at T_{C2} for the highest acid concentration.

Powder X-ray Diffraction. Powder X-ray diffractograms recorded as a function of the acid concentration are shown in Figure 2. First, for whatever the acid concentration, the diffractograms exhibit hexagonal ice Bragg peaks in addition to clathrate hydrate Bragg peaks. For example, this observation is confirmed by the PXRD pattern recorded at 150 K for α = 0 (corresponding to the ideal molar ratio for the type II THF clathrate hydrate[23]): the powder diffractograms are the superposition of the type II THF clathrate hydrate (i.e., cubic unit cell with a = 17.199 ± 0.008 Å at 150 K) with hexagonal ice (i.e., hexagonal unit cell with a = 4.508 ± 0.008 Å and c = 7.337 ± 0.008 Å at 150 K). Such structural signatures are in agreement with the double-peak shape associated with the melting of the sample at T_{C1} observed by means of DSC. The observations of the diffractograms vs the acid concentration lead to identify α = 0.125 as a specific point in terms of structural properties. For α smaller than 0.125, the Bragg peaks associated with the hydrate phase are indexed with the type II clathrate structure. For α greater than 0.125, additional Bragg peaks are observed, as shown by crosses in Figure 2. These additional diffraction peaks are indexed with the type I clathrate structure, which corresponds to the structure formed in the case of pure perchloric acid clathrate hydrate.[6] The diffractogram is then the superposition of two diffraction patterns (in addition to the ice phase): one associated with the type II structure and one associated with the type I structure. To confirm this observation, the temperature dependence of the diffractograms recorded for α = 0.5 is shown in Figure 3: the

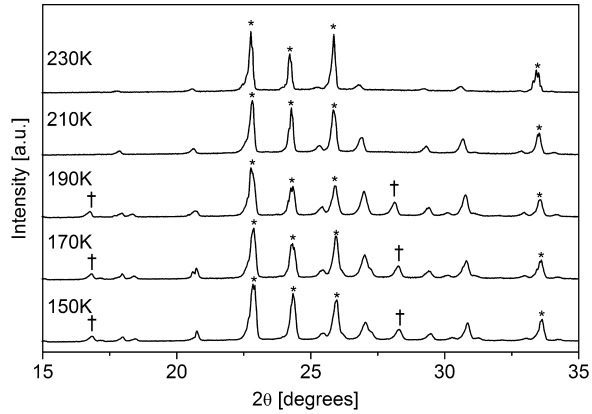

Figure 3. Diffractograms of the mixed THF−$HClO_4$ clathrate hydrates α = 0.5 for various temperatures. The peaks indicated with crosses correspond to the type I clathrate hydrate structure. The ice Bragg peaks are indicated with asterisks.

Bragg peaks associated with the type I structure vanish between 190 and 210 K (the diffractograms have been recorded in order of increasing temperatures). This behavior is in full agreement with the DSC peak T_{C2} observed at ca. 205 K (heating cycle in Figure 1). The thermal anomaly T_{C2} thus corresponds to the melting of the type I perchloric acid clathrate hydrate phase. The difference observed in the melting, with respect to the $HClO_4$·5.5 H_2O type I clathrate hydrate (melting at 228 K), is probably associated with a different hydration number for the type I of the present multiphase sample. Such a variation is

DOI: 10.1021/jp511826b
J. Phys. Chem. C 2015, 119, 8904−8911

known to occur in strong acid clathrate hydrates.[7] Moreover, for $\alpha > 0.125$, the type I diffraction signatures are slightly increasing with the acid concentration, but remain weak (see Figure 2). This variation suggests that the fraction of type I structure is negligible with respect to the one of type II structure in the sample. This observation is in agreement with the absence of thermal anomalies for $0.5 > \alpha > 0.125$ on the DSC curves (Figure 1).

The measured cell parameters of the type II clathrate phase are shown in Figure 4. With respect to the pure THF clathrate

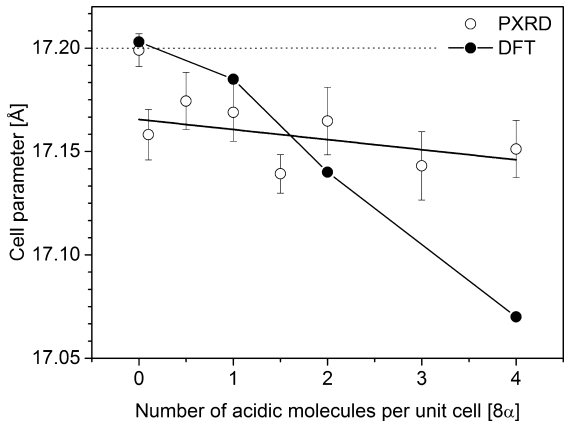

Figure 4. Measured cell parameter of the cubic type II unit cell of the mixed THF-$HClO_4$ clathrate hydrates at 150 K as a function of acid concentrations 8α.

hydrate ($a = 17.199 \pm 0.008$ Å at 150 K), the cell parameter of the type II mixed clathrate hydrate is smaller (the averaged value is $a = 17.16 \pm 0.01$ Å at 150 K). Such an effect has been also observed when doping THF clathrate hydrate with ammonium fluoride.[36] The shrinkage of the unit cell is a signature of perchlorate anions replacing the THF molecules (known to be located within the large cages[23]): the van der Waals volume of the ClO_4^- (V_{ClO_4}) anion is smaller than the one of the THF molecule (V_{THF}). Such observation suggests that the perchlorate anions are encapsulated within the large cage of the type II clathrate hydrate. Moreover, the cell parameter of the mixed clathrate hydrate does not significantly depend on the acid concentration (Figure 4). Together with the slight increase of the type I Bragg peaks for $\alpha > 0.125$ (Figure 2), such behaviors are indicative of a limited number of perchlorate anions that could be included within the type II THF clathrate hydrate. Thus, the perchlorate anions are preferentially included within the large cages of the type II THF clathrate hydrate with a concentration limit corresponding to $\alpha = 0.125$.

DFT Calculations. In order to complement the experimental findings, theoretical calculations using density functional theory (DFT) have been performed. The main purpose of these DFT calculations is to determine: (i) the shrinkage of type II unit cell observed in the X-ray diffraction experiments when perchloric acid is included; (ii) the influence of acid on the electrostatic interactions involved in the clathrate hydrate. These interactions include interactions between water molecules through hydrogen bonding (host−host interactions) and between the host cages and the guest molecule through possibly hydrogen bonding[37] and/or van der Waals interactions (guest−host interactions). When an acid is included in a cage, an ionic bonding could occur between a hydronium ion present in the aqueous substructure and the ClO_4^- anion. These electrostatic components may influence the stability of the clathrate hydrate.

As a starting point, the crystal parameter of the pure THF clathrate was calculated by relaxing the structure for different lattice constant a. The total free energy, that is of potential origin only (no kinetics contribution is considered in the calculations), is shown as a function of the cell parameters in Figure 5. The minimum energy has been found for $a = 17.203$

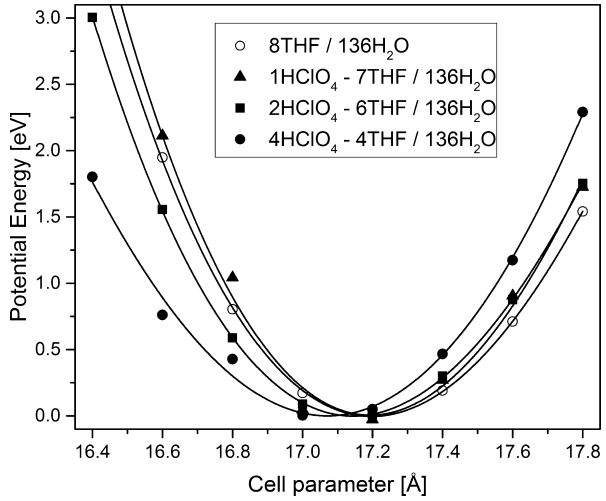

Figure 5. Potential energy of mixed clathrate hydrate from DFT calculations for various concentrations of $HClO_4$ acids (only the large cages are filled with guest molecules). The continuous lines represent the fitted curves with the help of the Birch−Murnaghan equation of state (see text for details).

Å that is close to the experimental value, as shown in Figure 4. For DFT calculations done without thermal energy, the theoretical result is within the error margin of calculations. The lattice constants determined for the mixed clathrate hydrate from Figure 5 are shown in Figure 4. A clear shrinkage effect of the unit cell volume with the increase of $HClO_4$ molecule is determined. Such an evolution is in qualitative agreement with the experiment PXRD results: the same behavior is observed between theoretical and experimental results, i.e., a decrease of a with the inclusion of perchloric acid, due to the difference of guest molecular volumes as previously mentioned ($V_{THF} > V_{ClO_4}$). Interestingly, theoretical results deviate from the experimental ones for the highest acid concentration; this should be related with the experimental observation of a multiphase system mixing type I and type II structures. Finally, it is worth noting that the determination of the bulk modulus, through a fitting of the curves in Figure 5 with the Birch−Murnaghan equation of state,[38] shows that on average this modulus decreases with insertion of acids. In other words, the insertion of acidic molecules leads to the increase of the elasticity for the ionic clathrate hydrate.

The investigation of the electrostatic interactions involved in the ionic clathrate hydrate stability may be done through the analysis of the nonbonding energy (i.e., energy not involved in covalent bonds), defined per molecule as

$$E_{NB} = (E_c - N_h E_h - N_g E_g)/(N_h + N_g)$$

where, N_h and N_g are respectively the number of host molecules (water molecules and hydronium ions) and the

DOI: 10.1021/jp511826b
J. Phys. Chem. C 2015, 119, 8904−8911

number of guest molecules (THF molecules and perchlorate anions), E_c is the total energy of the clathrate, E_h is the energy of the host molecule, and E_g is the energy of the guest molecule. Neglecting the guest−guest interaction in view of the intercage distance (almost 1 nm), the nonbonding energy contains information on host−host interactions (E_{HH}) and guest−host interactions (E_{GH}) since:

$$E_{NB} = (N_h E_{HH} + N_g E_{GH})/(N_h + N_g)$$

with

$$E_{HH} = (E_{ec} - N_h E_h)/N_h$$

and

$$E_{GH} = (E_c - E_{ec} - N_g E_g)/N_g$$

where E_{ec} is the energy of the clathrate without the guest molecule. As shown in Figure 6, the nonbonding energy

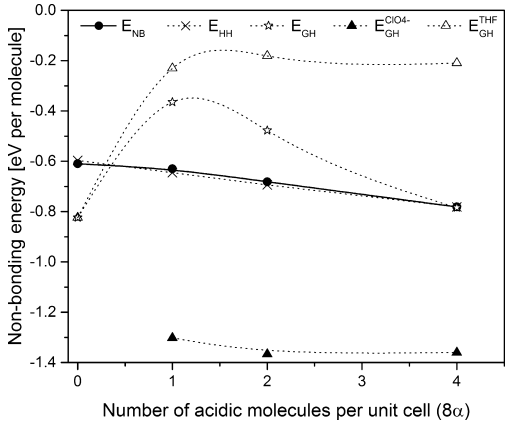

Figure 6. Evolution of nonbonding energy in the cubic type II unit cell of the mixed (1-α)THF·$\alpha$$HClO_4$·17$H_2O$ clathrate hydrates as a function of acid concentrations 8α (lines are a guide to the eyes). The total nonbonding energy E_{NB} is decomposed in host−host component E_{HH} and guest−host component E_{GH}. The guest−host nonbonding energy is decomposed into the perchlorate anion contribution $E_{GH}^{ClO_4^-}$ and the THF contribution E_{GH}^{THF}. The various curves are weighted by the number of molecular species (144 for total, 136 for E_{HH}, 8 for E_{GH}, 8α for $E_{GH}^{ClO_4^-}$ and 8(1-α) for E_{GH}^{THF}).

increases (in absolute value) with the number of acid molecules reflecting the fact that the insertion of acids stabilizes the electrostatic interactions in the hydrate. Regarding the contribution of host−host and guest−host interactions, it appears that the stabilization is mainly due to hydrogen bonding of the aqueous structure. Actually, this is an effect of the hydronium insertion that strongly contributes to the energetics of the system even at low concentration (four hydronium ions stabilize the system of about 0.2 eV/molecule). The guest−host energy curve presents a nonhomogeneous behavior that can be explained in Figure 6, where the total contribution has been decomposed in two contributions arising from the two kinds of guest molecules (THF and ClO_4^-). Clearly, the guest−host interactions are disrupted by the insertion of one acid molecule due to a destabilization of the THF−host interaction. The stronger ClO_4^- host interaction (ca. −1.3 eV/molecule against ca. −0.2 eV/molecule for THF−host) must strongly interfere with the aqueous substructure to lead to such a change in the THF−host energy. Introducing more acids molecules does not change the individual guest−host energies but contributes to the decrease of the total contribution as $E_{GH}^{ClO_4^-} < E_{GH}^{THE}$.

The energetic analysis brings two interesting types of information for this study. First, the stronger ClO_4^-−host interaction suggests that the cages containing an acid are compressed, in agreement with the volume shrinkage observed in Figure 4. Second, the greater stability of the electrostatic interactions of the ionic clathrate hydrate provides plausible evidence of the insertion of acid perchloric in the clathrate hydrates, as experimentally observed.

It is interesting to note that the strong destabilization of the THF−host interaction (ca. 0.6 eV/molecule) observed with the inclusion of one acid molecule could originate from the hydrogen bonding or van der Waals interaction. Nevertheless, the treatment of these later interactions could be improved by introducing an exchange correlation functional taking into account explicitly the long-range van der Waals interactions. More probably, hydrogen bonding should exist between THF and water cages to explain the large THF−host nonbonding energy (ca. 0.8 eV/molecule). Indeed, examination of the relaxed structure reveals the existence of host O−H bonds pointing toward the inner part of the cages. Thus, the presence of hydronium ions due to insertion of acid molecules should strongly interfere with the aqueous substructure leading to a possible explanation for the large destabilization of THF−host interaction via a large destabilization of the THF−host hydrogen bonding. The stronger ClO_4^- host interaction (ca. −1.3 eV/molecule against ca. −0.2 eV/molecule for THF−host) is probably due to ionic interactions between ClO_4^- and H_3O^+ ions. A deeper analysis of the electrostatic interactions would be required but is beyond the scope of this paper and will be the object of a future work.

Raman Scattering. The impact of the insertion of acidic molecules within the THF clathrate hydrate on vibrational properties has been investigated by means of Raman spectroscopy for the sample α = 0.125 with respect to the sample with α = 0. Raman spectra have been previously studied for the type II THF clathrate hydrate[39−41] and for the type I perchloric acid clathrate hydrate.[42,43] These studies allow the establishment of relevant Raman bands for investigating the mixed clathrate hydrate. The Raman peaks characteristic of the encapsulation of the guest molecules with in the clathrate cage are shown in Figure 7 at 210 K. The ring-breathing mode observed at 920 cm^{-1} is characteristic of the enclathrated THF molecule: with respect to aqueous THF solution, it is not split and its frequency is shifted.[40] The observed frequencies are identical in the pure THF clathrate hydrate and in the mixed THF−perchloric acid clathrate hydrate (Figure 7), confirming that the THF molecules are encapsulated in the large cage of the type II mixed clathrate hydrate. The totally symmetric stretching mode of the perchlorate anion is observed at 934 cm^{-1} in the perchloric acid clathrate hydrate (type I) and in the mixed perchloric acid−THF clathrate hydrate (type II). However, the frequency of this mode does not represent a characteristic signature of the encapsulation: there is no significant variation of its frequency in clathrate hydrate with respect to aqueous solution.[42,43]

The relevant signature of the perchlorate anions is associated with the mode ν_2 at 460.6 cm^{-1} and the mode ν_4 at 627 cm^{-1}. The ratio $R = I(\nu_4)/I(\nu_2)$ of the integrated intensities of the two modes constitutes a parameter characterizing the encapsulation of the perchlorate anions. In the $HClO_4$·5.5H_2O sample, the measured ratio is R = 0.947 ± 0.008

DOI: 10.1021/jp511826b
J. Phys. Chem. C 2015, 119, 8904−8911

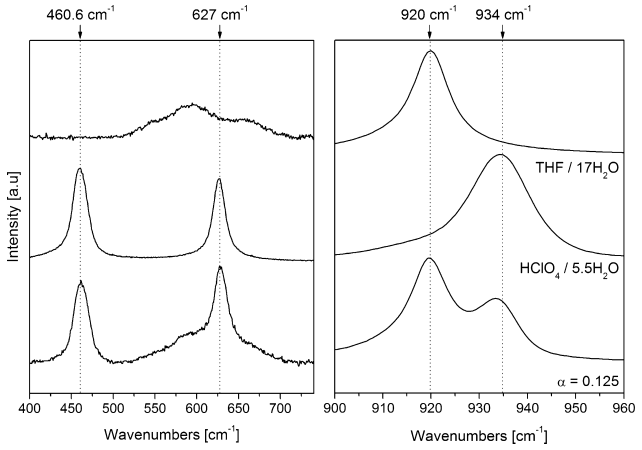

Figure 7. Regions of the Raman scattering characteristic of the encapsulated perchlorate anions (left) and of the encapsulated THF molecules (right) at 210 K. The intensities of the spectra on the left have been magnified.

(denoted R_{liq}) in its aqueous solution and $R = 0.322 \pm 0.005$ in its type I clathrate hydrate structure (denoted R_{typeI}). In the mixed clathrate hydrates, this ratio has been measured as a function of the acid concentration at 230 K (Figure 8), by

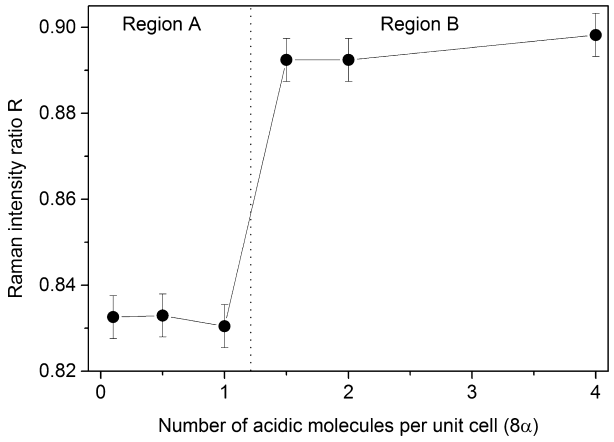

Figure 8. Acidic concentration dependence of the Raman intensity ratio of characteristic modes of perchlorate anions in the mixed clathrate hydrates at 230 K (see text for details).

subtracting the contribution of the THF ring-breathing mode[44] observed in the 600 cm^{-1} region (Figure 7). As observed in the structural analysis, the concentration $\alpha = 0.125$ represents a striking limit for the Raman signal: the ratio is $R = 0.893 \pm 0.006$ for $\alpha > 0.125$ (region B) and $R = 0.835 \pm 0.007$ for $\alpha \leq 0.125$ (region A). In the region B, the ratio (denoted R_B) is slightly smaller than R_{liq} since the measurement has been done above the melting of the perchloric acid clathrate hydrate: R_B then results from the superposition of the Raman intensities expected in the aqueous acidic solution (related to R_{liq}) with the Raman intensities expected for the mixed clathrate hydrate (denoted R_A). The R_A value corresponds to the one measured in the region A: as expected when the perchlorate anions are encapsulated in clathrate cages (for the type I structure, $R_{typeI} < R_{liq}$), the ratio R decreases for $\alpha \leq 0.125$ ($R = 0.835 \pm 0.007$). Thus, the Raman analysis confirms the encapsulation of the perchlorate anion within the cage of the THF clathrate hydrate with a maximum concentration corresponding to $\alpha = 0.125$.

Finally, the lattice mode region, corresponding to intermolecular O−O stretching of water molecules forming the clathrate cage,[40,45] is shown in Figure 9 at 230 K. As expected

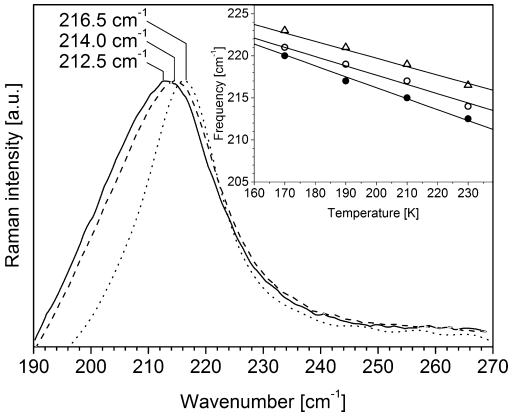

Figure 9. Translational lattice modes of the mixed clathrate hydrate $\alpha = 0.125$ (continuous line), of THF clathrate hydrate (dashed line) and of ice I_h (dotted line) at 230 K. The inset shows the thermal evolution of the lattice frequencies for the mixed clathrate hydrate (filled circles), the THF clathrate hydrate (open circles), and the ice (triangles).

this lattice mode is observed at lower frequency in the THF clathrate hydrate (214 cm^{-1}) with respect to the ice (216.5 cm^{-1}) at 230 K. In the case of the mixed clathrate hydrate, this mode is further lowered to 212.5 cm^{-1} at 230 K. As shown in Figure 9, this behavior is systematically observed in the studied temperature region. This feature represents a signature of the softening of the lattice mode by adding acidic molecules within the THF clathrate hydrate. In other words, the addition of acidic protons within the host H-bond network modifies the flexibility of the cage. Such observation is in full agreement with the DFT calculations, showing that the replacement of THF molecules by acidic molecules in the large cage of the type II clathrate hydrate changes the elasticity of the structure.

CONCLUDING REMARKS

New clathrate hydrates have been synthesized through the substitution of THF molecules with perchlorate anions within the cationic type II cage structure. The impact of these acidic additives has been investigated onto the calorimetric, structural, and vibrational properties of the mixed clathrate hydrate, prepared with $(1-\alpha)THF{\cdot}\alpha HClO_4{\cdot}17H_2O$ solutions (α varying between 0 and 1/2). The combination of DSC, PXRD, Raman scattering, and computational structure relaxation in the DFT approximation yield a complete description of the mixed clathrate hydrate in terms of type II structure. Within the cationic host substructure, the large cages are preferentially filled with either THF molecules or perchlorate anions, leaving the small cage most probably empty (Figure 10). An inherent limitation exists of the concentration of acidic species within the type II structure: a solution containing no more than one acidic molecule for seven THF molecule can be used to form a single type II clathrate phase (i.e., $\alpha < 0.125$). Above this limit, a multiphasic behavior is observed, so that the clathrate phase is constituted of a mixture of type I and type II structures. In the monophasic regime, the melting and fusion points strongly depend on the acid concentration. Such a chemical substitution thus offers the opportunity to modify the thermodynamic

DOI: 10.1021/jp511826b
J. Phys. Chem. C 2015, 119, 8904−8911

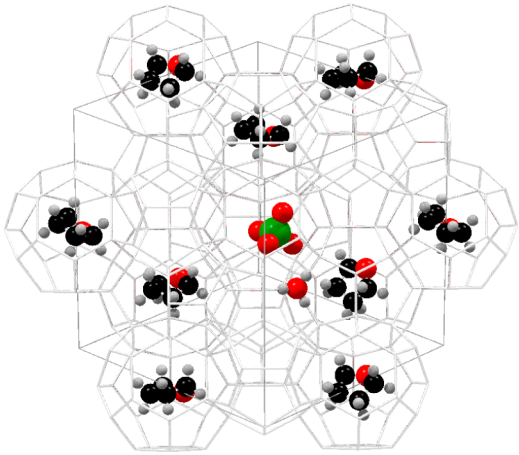

Figure 10. Structural representation of the cages forming the DFT-relaxed $7THF{\cdot}1HClO_4{\cdot}136H_2O$ clathrate hydrates (type II cubic unit cell with a = 17.185 Å). While all small 5^{12} cages are empty, the large $5^{12}6^4$ cages are filled with either perchlorate anion (middle; maximum of one anion per unit cell) or THF molecules. The hydronium cation participating to the cage substructure is also represented (water molecules are not represented for clarity).

properties of the THF clathrate hydrate, by conserving the clathrate structure.

With the help of PXRD and DFT structure relaxation, the analysis of the cell parameters obtained in the monophasic domain reveals the shrinkage of the unit cell in the mixed clathrate hydrate compared with the pure THF clathrate hydrate. Such a structural feature constitutes evidence of the insertion of perchlorate anions within the large cages of the type II structure: the van der Waals volume of the ClO_4^- (V_{ClO_4}) anion is smaller than the one of the THF molecule (V_{THF}). The influence of acid on the electrostatic interactions involved in the clathrate hydrate was investigated with the help of the DFT calculations. The compression of the large cages containing acidic species compared to the one containing THF molecules is a direct signature of the strong ionic character of the guest–host interaction. Moreover, the nonbonding energy is decreased when acidic ions are introduced within the type II unit cell. The acidic additives thus stabilized the type II structure, in terms of electrostatic interactions.

The energetic analysis of the DFT structure relaxation and the low frequency mode analysis of the Raman scattering reveal that the insertion of acidic species within the THF clathrate hydrate generates a softening of the host substructure. Such a result is counterintuitive in the frame of the harmonic approximation. Indeed, the shrinkage of the unit cell may be associated with the decrease of the intermolecular distance: this contraction should result in the hardening of the lattice mode, in contradiction with the experimental and theoretical observations. On one hand the host–guest interaction is involved in the shrinkage phenomenon, as reflected by the strong anion–host nonbonding energy calculated by means of DFT. On the other hand, the inclusion of hydronium cations within the host substructure strongly modifies the intermolecular potential linked to the H-bonding network. This latter point may be related to the potential shape or to its anharmonicity (in this issue, DFT calculations may be improved by treating the van der Waals interactions with the help of nonlocal exchange-correlation functional, the object of a future work). The present work illustrates the knowledge of the existing competition between these two contributions.[46,47] Such a question is clearly open and the present study brings new experimental evidence about the importance of the ionic defects in the stability of clathrate hydrates.

AUTHOR INFORMATION

Corresponding Author

*E-mail: a.desmedt@ism.u-bordeaux1.fr. Phone: ++33 5 4000 2937. Fax: ++33 5 4000 6994.

Notes

The authors declare no competing financial interest.

ACKNOWLEDGMENTS

This paper falls into the frame of the project ANR 2011-JS08-002-01, funded by the French ANR "Agence Nationale de la Recherche". The high performance center IDRIS, funded by the French National Centre for Scientific Research (CNRS), is thanked for allocating computing time. With the help of P. Aurel, calculations have also been carried out on the "Mésocentre de Calcul Intensif Aquitaine" (MCIA), granted by the Conseil Régional d'Aquitaine and the French Ministry of Research and Technology. J. L. Bruneel and D. Talaga are thanked for their technical assistance during the Raman scattering experiments performed on equipment of the Vibrational Spectroscopy and Imaging (SIV at ISM) platform, funded by the "Conseil Régional d'Aquitaine" and Europe (FEDER programme).

REFERENCES

(1) Jeffrey, G. A., Hydrate Inclusion Compounds. In *Comprehensive Supramolecular Chemistry*; Atwood, J. L., Davies, J. E. D., Mac-Nicol, D. D., Vögtle, F., Eds; Pergamon: Oxford, UK, 1996; Vol. *6*, p 757.

(2) Sloan, E. D.; Koh, C. A. *Clathrate Hydrates of Natural Gases*, 3rd ed.; Taylor & Francis-CRC Press: Boca Raton, FL, 2008.

(3) Sum, A. K.; Koh, C. A.; Sloan, E. D. Clathrate Hydrates: From Laboratory Science to Engineering Practice. *Ind. Eng. Chem. Res.* **2009**, *48*, 7457–7465.

(4) Shin, K.; Cha, M.; Choi, S.; Dho, J.; Lee, H. Discrete Magnetic Patterns of Nonionic and Ionic Clathrate Hydrates. *J. Am. Chem. Soc.* **2008**, *130*, 17234–17235.

(5) Desmedt, A.; Bedouret, L.; Pefoute, E.; Pouvreau, M.; Say-Liang-Fat, S.; Alvarez, M. Energy Landscape of Clathrate Hydrates. *Eur. Phys. J. (Special Topics)* **2012**, *213*, 103–127.

(6) Mootz, D.; Oellers, E.-J.; Wiebke, M. First Examples of Type I Clathrate Hydrates of Strong Acids: Polyhydrates of Hexafluorophosphoric, Tetrafluoroboric, and Perchloric Acid. *J. Am. Chem. Soc.* **1987**, *109*, 1200–1202.

(7) Cha, J.; Shin, K.; Choi, S.; Lee, S.; Lee, H. Maximized Proton Conductivity of the HPF_6 Clathrate Hydrate by Structural Transformation. *J. Phys. Chem. C* **2008**, *112*, 13332–13335.

(8) Bode, V.; Teufer, G. Die Kristallstruktur der Hexafluorophosphorsäure. *Acta Crystallogr.* **1955**, *8*, 611–614.

(9) Yamamuro, O.; Oguni, M.; Matsuo, T.; Suga, H. Calorimetric Study of Pure and KOH-Doped Tetrahydrofuran Clathrate Hydrate. *J. Phys. Chem. Solids* **1988**, *49*, 425–434.

(10) Sangwai, J. S.; Oellrich, L. Phase Equilibrium of Semiclathrate Hydrates of Methane in Aqueous Solutions of Tetra-n-butyl Ammonium Bromide (TBAB) and TBAB–NaCl. *Fluid Phase Equilib.* **2014**, *367*, 95–102.

(11) Borkowska, Z.; Tymosiak, A.; Opallo, M. Conductivity of Stoichiometric $(CH_3)_4NOH$ Clathrate Hydrates. *J. Electroanal. Chem.* **1996**, *406*, 109–117.

(12) Opallo, M.; Tymosiak, A.; Borkowska, Z. Conductivity of Tetramethylammonium Fluoride Tetrahydrate. *J. Electroanal. Chem.* **1995**, *387*, 47–52.

DOI: 10.1021/jp511826b
J. Phys. Chem. C 2015, 119, 8904–8911

(13) Cappadonia, M.; Kornyshev, A. A.; Krause, S.; Kuznetsov, A. M.; Stimming, U. Low-Temperature Proton Transport in Clathrates. *J. Chem. Phys.* **1994**, *101*, 7672−7682.
(14) Huang, T.-H.; Davis, R. A.; Frese, U.; Stimming, U. Proton Mobility in Liquid and Frozen $HClO_4$-5.5H_2O: NMR and Conductivity Measurements. *J. Phys. Chem.* **1988**, *92*, 6874−6876.
(15) Aschrafi-Mahabadi, S.; Cappadonia, M.; Stimming, U. Proton Transport in Solid Electrolytes with Clathrate Structure. *Solid State Ionics* **1994**, *70/71*, 311−315L.
(16) Bedouret, L.; Judeinstein, P.; Ollivier, J.; Combet, J.; Desmedt, A. Proton Diffusion in the Hexafluorophosphoric Acid Clathrate Hydrate. *J. Phys. Chem. B* **2014**, *118*, 13357−13364.
(17) Desmedt, A.; Stallmach, F.; Lechner, R. E.; Cavagnat, D.; Lassegues, J. C.; Guillaume, F.; Grondin, J.; Gonzalez, M. A. Proton Dynamics in the Perchloric Acid Clathrate Hydrate $HClO_4$-5.5H_2O. *J. Chem. Phys.* **2004**, *121*, 11916−11926.
(18) Desmedt, A.; Lechner, R. E.; Lassègues, J. C.; Guillaume, F.; Cavagnat, D.; Grondin, J. Hydronium dynamics in the perchloric acid clathrate hydrate. *Solid State Ionics* **2013**, *252*, 19−25.
(19) Krivchikov, A. I.; Romantsova, O. O.; Korolyuk, O. A. The Effect of Proton Ordering on the Thermal Conductivity of Clathrate Tetrahydrofuran Hydrate. *Low Temp. Phys.* **2008**, *34*, 648−654.
(20) Cha, M.; Shin, K.; Kwon, M.; Koh, D. Y.; Sung, B.; Lee, H. Superoxide Ions Entrapped in Water Cages of Ionic Clathrate Hydrates. *J. Am. Chem. Soc.* **2010**, *132*, 3694−3696.
(21) Shin, K.; Cha, M.; Lee, W.; Kim, H.; Jung, Y.; Dho, J.; Kim, J.; Lee, H. Superexchange-Like Interaction of Encaged Molecular Oxygen in Nitrogen-Doped Water Cages of Clathrate Hydrates. *J. Am. Chem. Soc.* **2011**, *133*, 20399−20404.
(22) Shin, K.; Cha, M.; Lee, W.; Seo, Y.; Lee, H. Abnormal Proton Positioning of Water Framework in the Presence of Paramagnetic Guest within Ion-Doped Clathrate Hydrate Host. *J. Phys. Chem. C* **2014**, *118*, 15193−15199.
(23) Mak, T. C.; McMullen, R. K. Polyhedral Clathrate Hydrates. X. Structure of Double Hydrate of Tetrahydrofuran and Hydrogen Sulfide. *J. Chem. Phys.* **1965**, *42*, 2732−2737.
(24) Jones, C. Y.; Marshall, S. L.; Chakoumakos, B. C.; Rawn, C. J.; Ishii, Y. Structure and Thermal Expansivity of Tetrahydrofuran Deuterate Determined by Neutron Powder Diffraction. *J. Phys. Chem. B* **2003**, *107*, 6026−6031.
(25) Dong, C. PowderX: Windows-95-based Program for Powder X-ray Diffraction Data Processing. *J. Appl. Crystallogr.* **1999**, *32*, 838.
(26) The Software Program Chekcell is available on the web. Developed by Laugier, L.; Bochu, B. Laboratoire des Materiaux et du Genie Physique, Ecole Superieure de Physique de Grenoble.
(27) Kresse, G.; Hafner, J. Ab Initio Molecular Dynamics for Liquid Metals. *Phys. Rev. B* **1993**, *47*, 558−561.
(28) Kresse, G.; Furthmüller, J. Efficiency of Ab-Initio Total Energy Calculations for Metals and Semiconductors Using a Plane-Wave Basis Set. *Comput. Mater. Sci.* **1996**, *6*, 15−50.
(29) Perdew, J. P.; Burke, K.; Ernzerhof, M. Generalized Gradient Approximation Made Simple. *Phys. Rev. Lett.* **1996**, *77*, 3865−3868.
(30) Blöchl, P. E. Projector Augmented-Wave Method. *Phys. Rev. B* **1994**, *50*, 17953−17979.
(31) Kresse, G.; Joubert, J. From Ultrasoft Pseudopotentials to the Projector Augmented-Wave Method. *Phys. Rev. B* **1999**, *59*, 1758−1775.
(32) Zhang, Y.; Debenedetti, P. G.; Prud'homme, R. K.; Pethica, B. A. Differential Scanning Calorimetry Studies of Clathrate Hydrate Formation. *J. Phys. Chem. B* **2004**, *108*, 16717−16722.
(33) Tombari, E.; Presto, S.; Salvetti, G.; Johari, G. P. Heat Capacity of Tetrahydrofuran Clathrate Hydrate and of its Components, and the Clathrate Formation from Supercooled Melt. *J. Chem. Phys.* **2006**, *124*, 154507(1−10).
(34) Lehmkühler, F.; Sakko, A.; Sternemann, C.; Hakala, M.; Nygård, K.; Sahle, C. J.; Galambosi, S.; Steinke, I.; Tiemeyer, S.; Nyrow, A.; Buslaps, T.; Pontoni, D.; Tolan, M.; Hämäläinen, K. Anomalous Energetics in Tetrahydrofuran Clathrate Hydrate Revealed by X-ray Compton Scattering. *J. Phys. Chem. Lett.* **2010**, *1*, 2832−2836.
(35) Lehmkühler, F.; Sakko, A.; Stinke, I.; Sternemann, C.; Hakala, M.; Sahle, C. J.; Buslaps, T.; Simonelli, L.; Galambosi, S.; Paulus, M.; Pylkkänen, T.; Tolan, M.; Hämäläinen, K. Temperature-Induced Structural Changes of Tetrahydrofuran Clathrate and of the Liquid Water/Tetrahydrofuran Mixture. *J. Phys. Chem. C* **2011**, *11*, 21009−21015.
(36) Shin, K.; Moudrakovski, I. L.; Davari, M. D.; Alavi, S.; Ratcliffe, C. I.; Ripmeester, J. A. Crystal Engineering the Clathrate Hydrate Lattice with NH_4F. *Cryst. Chem. Eng.* **2014**, *16*, 7209−7217.
(37) Alavi, S.; Ripmeester, J. A. Effect of Small Cage Guests on Hydrogen Bonding of THF in Binary Structure II Clathrate Hydrates. *J. Chem. Phys.* **2012**, *137*, 054712(1−7).
(38) Birch, F. Finite Elastic Strain of Cubic Crystals. *Phys. Rev.* **1947**, *71*, 809−824.
(39) Tulk, C. A.; Klug, D. D.; Ripmeester, J. A. Raman Spectroscopic Studies of THF Clathrate Hydrate. *J. Phys. Chem. A* **1996**, *102*, 8734−8739.
(40) Prasad, P. S. R.; Shiva Prasad, K.; Thakur, N. K. Laser Raman Spectroscopy of THF Clathrate Hydrate in the Temperature Range 90−300 K. *Spectrochimica Acta Part A* **2007**, *68*, 1096−1100.
(41) Subramanian, S.; Sloan, E. D. Trends in Vibrational Frequencies of Guests Trapped in Clathrate Hydrate Cages. *J. Phys. Chem. B* **2002**, *106*, 4348−4355.
(42) Karelin, A. I. Solid Solutions, Clathrate Structures, and Vibrational Spectra of Plastic Crystals of $HClO_4$·5.5H_2O. *J. Struct. Chem.* **1991**, *32*, 199−208.
(43) Ratcliffe, C. I.; Irish, D. E. Vibrational Spectral Studies of Solutions at Elevated Temperatures and Pressures. VI. Raman Studies of Perchloric Acid. *Can. J. Chem.* **1984**, *62*, 1134−1144.
(44) Cadioli, B.; Gallinella, E.; Coulombeau, C.; Berthier, G. Geometric Structure and Vibrational Spectrum of Tetrahydrofuran. *J. Phys. Chem.* **1993**, *97*, 7844−7856.
(45) Klobes, B.; Desmedt, A.; Sergueev, I.; Schmalzl, K.; Hermann, R. P. ^{129}Xe Nuclear Resonance Scattering on Solid Xe and ^{129}Xe Clathrate Hydrate. *EPL* **2013**, *103*, 36001(1−6).
(46) Chazallon, B.; Itoh, H.; Koza, M.; Kuhs, W. F.; Schober, H. Anharmonicity and Guest−Host Coupling in Clathrate Hydrates. *Phys. Chem. Chem. Phys.* **2002**, *4*, 4809−4816.
(47) Schober, H.; Itoh, H.; Klapproth, A.; Chihaia, V.; Kuhs, W. F. Guest-Host Coupling and Anharmonicity in Clathrate Hydrates. *Eur. Phys. J. E* **2003**, *12*, 41−49.

DOI: 10.1021/jp511826b
J. Phys. Chem. C 2015, 119, 8904−8911